Journal of Thermal Science Vol.32, No.3 (2023) 1263−1277

https://doi.org/10.1007/s11630-023-1792-0 **Article ID: 1003-2169(2023)03-1263-15**

Effects of the Secondary Air Excess Ratio on the Self-Preheating Combustion Characteristics and NO_x Emission of Semi-Coke

DING Hongliang[1,2], OUYANG Ziqu[1,2*], CAO Xiaoyang[1], ZHU Shujun[1]

1. Institute of Engineering Thermophysics, Chinese Academy of Sciences, Beijing 100190, China
2. University of Chinese Academy of Sciences, Beijing 100049, China

Abstract: The effects of the secondary air excess ratio (λ_2) on the self-preheating combustion characteristics and NO_x emission of semi-coke have been experimentally studied on a bench-scale test rig. Flameless combustion of the high-temperature preheated fuel (coal gas & coal char) has been achieved in all experimental cases. Through fire-observation windows, the combustion zone was transparent and no flame fronts were seen. Additionally, different λ_2 in this study were basically within the common range of self-preheating combustion technology. The results manifested that the rapid ignition of coal gas and the recirculation of high-temperature flue gas resulted in relatively high combustion temperatures close to the secondary air nozzle exit. With the increase of λ_2, the unburned carbon content of fly ash increased slightly and combustion efficiencies of all experiments exceeded 98%. Moreover, the exit NO_x emission was not reduced linearly, which was dissimilar from conventional air staging combustion. The main reason was that the volatile-N was released in the self-preheating device, and the air staging method could not effectively reduce the char-NO_x. In the course of the experiments, the lowest NO_x emission was 64.35 mg/m^3 (@6%O_2) when λ_2 was 0.40.

Keywords: self-preheating, pulverized coal, NO_x emission, flameless combustion

1. Introduction

Seriously damaging the atmospheric environment and endangering the health of humankind, NO_x is a highly toxic pollutant and the causation of acid rain and photochemical smog [1, 2]. NO_x emission from the burning of coal in thermal power plants has caught public's eyes for a long period. Since the 1970s, developed countries in Europe and America have formulated their own NO_x emission evaluating indicators successively, which have become increasingly strict [3]. In 2015, National Development and Reform Commission and National Energy Administration of China jointly put forward the ultra-low emission standard for NO_x of coal-fired power generating units in the combustion process: the emission of NO_x shall not exceed even 50 mg/m^3 (@6%O_2) [4]. In the face of the severe environmental situation and low pollution emission standards, it has become imperative to explore more effective NO_x reduction technologies and methods [5].

To tackle the issue of NO_x emissions in fossil fuel combustion, quite a few technologies have been proposed by the researchers. Among those proposals, the most widely deployed de-NO_x technology is air staging combustion technology. By air staging, the fuel is first burnt under oxygen-lean conditions to curb the formation

Received: Mar 4, 2021 AE: CHEN Zheng Corresponding author: OUYANG Ziqu E-mail: ouyangziqu@iet.cn

of NO_x, and subsequently the remaining combustion air is introduced at a suitable port downstream of the combustor to ensure efficient combustion of the fuel. This method plays an effective role in shrinking NO_x emission in pulverized coal combustion and has been widespreadly used for coal-fired power plants. Therefore, a mass of researchers conducted in-depth research on air staging and proposed different air staging forms [6–9]. However, the average original NO_x emission level of coal-fired units is still about 200–400 mg/m^3 (@6%O_2) [10]. Lower NO_x emissions can only be achieved by using secondary denitration technology such as selective non-catalytic reduction (SNCR) technology [11], selective reduction (SCR) technology [12], etc. Additionally, the combustion of fuel in the first stage combustion zone is carried out at a lower than theoretical air volume, which will generate numerous incomplete combustion products, thus reducing the combustion efficiency and inducing a greater potential for slagging and corrosion [13]. As a result, it is quite necessary to reasonably organize air staging combustion with the aim of reducing NO_x emissions and ensuring higher economy and reliability of boiler combustion at the same time.

In comparison with conventional combustion technologies, flameless combustion (MILD), as a new nitrogen-reducing combustion technology, has been favored by many researchers and developed rapidly in recent 30 years, characterized by uniform temperature profile, invisible flame front and low peak temperature. Table 1 shows investigations of the flameless combustion of solid fuels (coal or residual char) in chronological order over the past decade. The research methods are mainly divided into numerical simulation and experiment. Stadler et al. [14] carried out experiments on NO_x emission during coal combustion and found that NO_x generation from flameless oxy-fuel combustion of pulverized coal was fuel NO, and there was a certain difference with regard to the conversion rate of fuel-N to NO and the reduction effect of NO re-burning in case of oxy-fuel combustion in comparison with combustion in air atmosphere. Additionally, Vascellari et al. [15] investigated the influence of turbulence-chemistry interaction on CFD pulverized coal MILD combustion modeling, and found that the macro simulation result of Eddy Dissipation Concept (EDC) was more consistent with the trial value, and the prediction of turbulent chemical interactions was more accurate at a micro scale. In the simulation research of flameless combustion, Mei et al. [16] found that when the introduced primary air was parallel to or deviated from the secondary air, an increase in primary air velocity could help achieve flameless combustion, but excessive velocity might damage the fuel-enriched combustion zone and oxygen-enriched combustion zone generated by the separation of the primary air and the secondary air, resulting in a high-temperature area. What's more, Li et al. [17] and Smart et al. [18] defined the flameless combustion of solid fuels (pulverized coal), namely the burning of volatiles did not yield any yellow flame or was invisible, while visible sparks might exist. Mei et al. [19] adopted numerical method to study the effects of fuel injection angle (α) and the separation distance of primary and secondary air nozzles (S) on flameless combustion of pulverized coal in a pilot-scale furnace. The results revealed that NO emission decreased with the increase of α and S. Moreover, Weidmann et al. [20] researched flameless combustion of pulverized coal in a 500 kW pilot-scale furnace, observing that the flame during MILD combustion consisted of the visible spark of pulverized coal and the flame of volatiles with invisible front. In the simulation research of flameless combustion based on a 60 kW furnace, Saha et al. [21, 22] found that the increase of O_2 concentration and jet Reynolds number would result in increased precipitation rate of volatiles. Furthermore, the increased jet Reynolds number would also reduce the total carbon consumption rate. In a 0.30 MW down-fired pilot-scale furnace, Mao et al. [23, 24] also observed that the combustion area presented dark red without visible flame front and found that the burnout ratio of pulverized coal was reduced under flameless combustion. Saha et al. [25] studied the effects of particle size on flameless combustion characteristics of brown coal based on experiment and numerical values. The results suggested that the devolatilization time of small particles was earlier than that of large particles, which was believed that such difference was related to the dispersion of particles in the jet and difference of Stokes number. Perrone et al. [26] conducted some numerical simulations to analyze the feasibility of combining flameless combustion and oxy-combustion. The results demonstrated that the flameless oxy-combustion could inhibit the generation of NO_x and strengthen the recirculation, which favored the NO_x re-burning route. Hu et al. [27] systematically researched combustion characteristics of residual char on a 300 kW pilot-scale test rig. The results revealed that the flameless combustion of residual char was feasible under the condition of the non-preheating secondary air. In addition, flameless combustion could achieve low NO_x emission and high burnout ratio, serving as an effective means for large scale utilization of residual char. In the simulation research of flameless combustion of pulverized coal mixed with biomass, Wang et al. [28] found that both oxy-fuel combustion and biomass-mixed combustion could help reduce NO_x emission from pulverized coal flameless combustion. Furthermore, when the proportion of biomass was increased from 0% to 30%, NO_x emission from flameless combustion (air)

Table 1 Investigations of the flameless combustion of solid fuels

Year	Fuel	Oxidant	Oxidant temperature	Factor	Methodology	Reference
2011	Coal	Air and oxy-fuel	N/A	Effect of O_2 concentration	Experiment	[14]
2012	Coal	Air	1623 K	Influence of turbulence-chemical interaction	CFD	[15]
2012	Coal	Oxy-fuel	N/A	Flameless combustion tests under oxy-fuel conditions	Experiment	[18]
2014	Coal	Air	1623 K	Influences of reactant injection velocities	CFD	[16]
2014	Light oil and coal	Air and oxy-fuel	450 K	Global characteristics in a plot-scale furnace	Experiment	[17]
2015	Coal	Air	1623 K	Effect of the fuel injection angle and the separation distance of the primary-secondary air nozzle	CFD	[19]
2016	Coal	Air	417–422 K	Detailed measurement	Experiment	[20]
2016	Coal	Air	1284 K	Effect of turbulence	Experiment	[21]
2017	Coal	Air	373 K, 500 K	MILD combustion under low preheating temperature	Experiment	[23]
2017	Coal	Air	1284 K	Effect of particle size	Experiment	[25]
2017	Coal	Oxy-fuel	525 K	Coal MILD-oxy combustion integrated with flue gas recirculation	Experiment	[24]
2018	Coal	Oxy-fuel	850 K	Flameless-oxy combustion	CFD	[26]
2019	Residual char	Air	288 K	NO emission in a pilot-scale furnace	Experiment	[27]
2019	Coal	O_2	325 K	Effect of co-flow oxygen concentration	Experiment and CFD	[22]
2020	Biomass and coal	Air	1623 K	Effect of biomass co-firing ratio	CFD	[28]
2020	Coal	Air and oxy-fuel	1623 K	Effect of oxygen level	CFD	[29]

was reduced by 73×10^{-6} and that from flameless combustion (oxy-fuel) was reduced by 141×10^{-6}. Kuang et al. [29] numerically studied the MILD-oxy combustion characteristics of pulverized coal with oxygen concentrations from 10% to 50%, and found that under flameless oxy-combustion, increasing O_2 concentration could promote the gasification reaction between the char and CO_2, which would have a significantly impact on CO emission.

From previous flameless studies, it can be seen that the researches on flameless combustion of solid fuel mainly attached importance to the heterogeneous fuel NO formation, combustion reaction and the highly preheated air condition. Nevertheless, the information about how to achieve flameless combustion of high-temperature preheated coal char and the corresponding NO_x emission control strategy is fairly limited.

At present, high temperature air combustion (HTAC) is the main way to achieve flameless combustion of solid fuel. The high temperature and low oxygen air [30, 31] produced by gas combustion or heat storage body is used as combustion assistant air to realize flameless combustion which the high speed jet of ambient air is also used to absorb the high-temperature flue gas to realize [32, 33]. In the 1980s, All-Russian Thermal Engineering Institute proposed a technology of heating pulverized coal [34, 35]. NO_x emission produced by coal combustion was greatly reduced after the pulverized coal was heated by natural gas. Nevertheless, the existence of external heat source made the system structure more complicated. Inspired by HTAC technology, the Institute of Engineering Thermophysics, Chinese Academy of Sciences (IET, CAS) proposed a brilliant and promising combustion technique, by the virtue of which, the coal could be preheated by its partial combustion in a self-preheating device. Therefore, other heat resources were unnecessary. The main idea of self-preheating combustion technology is that the concentrated pulverized coal airflow with a chemical equivalence ratio far less than 1.00 is partially burned in a self-preheating device in advance with most volatiles separated out, and the combustion products subsequently enter a combustor for low-nitrogen combustion. Experimental researches relevant to this technique for anthracite, semi-coke and coal gasification fly ash were initiated in bench-scale test rigs [36–39] and pilot-scale test rigs [40, 41]. The denitration performance of this technology was demonstrated both stable and reliable. In other words, self-preheating combustion technology opened up a new path of fuel-N directional conversion, and realized the inhibition of NO_x generation in situ combustion reactions, thus providing a good application prospect.

With the advancement of self-preheating combustion technology, the secondary air distribution mode and nozzle optimization, which are significant factors that affect NO_x emission generated by coal combustion, are attached more and more importance to Refs. [42–44]. Based on this, the secondary air excess ratio is particularly vital. However, there are few pieces of reports related to the adoption of self-preheating combustion technology to study the efficient and clean combustion of semi-coke under different secondary excess air ratios. On the basis of previous studies [37, 43, 44], self-preheating combustion technology has been employed in this study and the flameless combustion of Shenmu semi-coke has been realized in the combustor, in an attempt to explore whether the combination of flameless combustion technology and air staging combustion technology could be attributive to further reduce NO_x emission in pulverized coal combustion. Simultaneously, the effects of the key parameter (λ_2) on the flameless combustion characteristics of the high-temperature preheated fuel and NO_x emission were intensively studied.

2. Experimental

2.1 Experimental setup

The experimental facility has been reached an exhaustive description in the literature [45] which was primarily constituted of a self-preheating device and a down-fired combustor (DFC) as revealed in Fig. 1. The main feature was that the high-temperature preheated fuel was obtained in the self-preheating device with low excess air ratio at the very beginning, and could be sent into the DFC for complete combustion thereafter.

The inner diameter and the height of the CFB riser, on the side of which there was a feed inlet port fed by a screw feeder, were respectively 90 mm and 1500 mm. The operating fluidized velocity was about 1.3–2.5 m/s. An electric heater was installed at the bottom of the riser with the purpose of heating the bed material in the course of start-up, and it would be turned off after the self-preheating device operated stably. A sampling port was arranged at the self-preheating device outlet for collecting the high-temperature coal gas that was

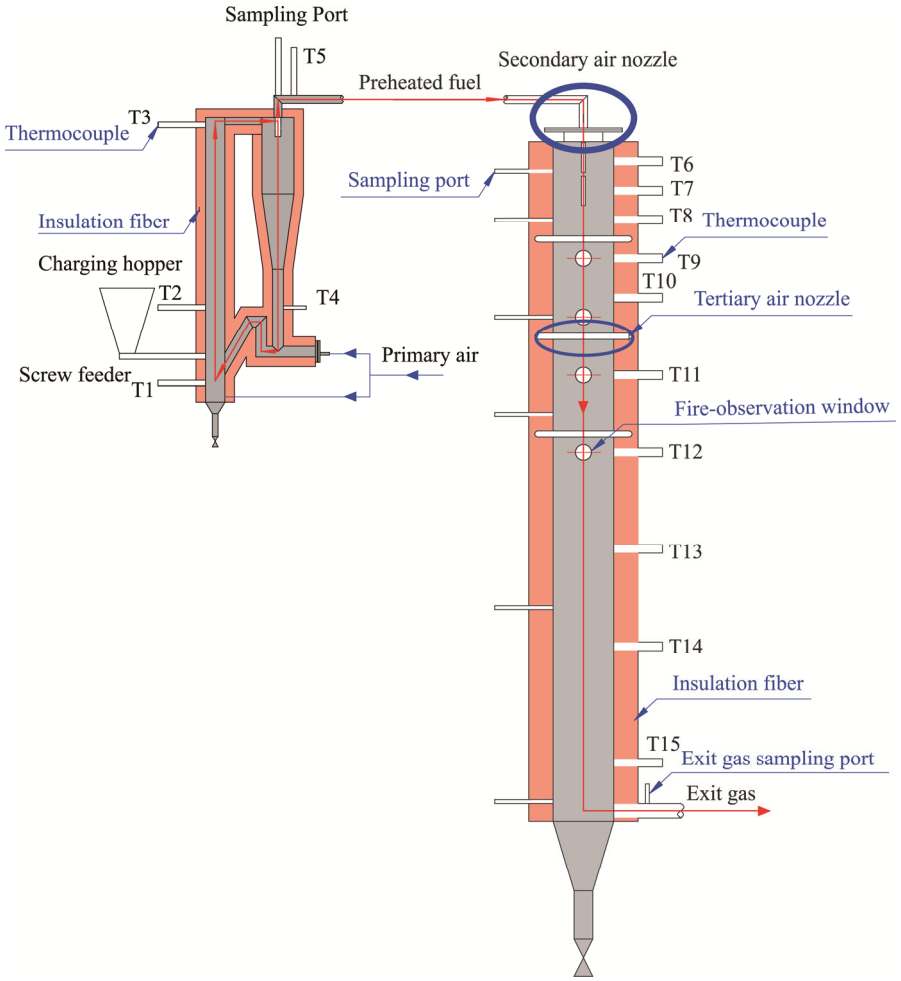

Fig. 1 Schematic diagram of the experimental facility

primarily constituted by N_2, CO, CO_2, H_2 and CH_4, and accompanying high-temperature coal char. The entire self-preheating device was covered with insulation cotton with a thickness of about 100 mm to help minimize the heat loss.

The inner diameter and the height of the down-fired combustor (DFC) made of Cr25Ni20 stainless steel were respectively 300 mm and 3500 mm. To provide the needed air to burn off the fuel, there were three layers of the tertiary air nozzle installed on the side wall of the DFC and located at 500 mm, 1000 mm and 1500 mm respectively. The schematic diagram of tertiary air nozzle was shown in Fig. 2. To observe the burning condition of the flame, there were six fire-observation windows on the side wall of the DFC respectively located at 80 mm, 250 mm, 600 mm, 900 mm, 1200 mm and 1600 mm. Among them, the top two were 15 mm×150 mm square, and the remaining four were circular with the inner diameter of 63 mm. In consideration of ash accumulation in fire-observation windows, a minor amount of compressed air was introduced to purge the dust stratification. For the sake of the extremely insignificant total amount which was given rise to infrequent supply in the experiment, the influence of this part of compressed air would not be taken into consideration in this study. The entire DFC was also covered with insulation cotton of about 100 mm thick for heat insulation.

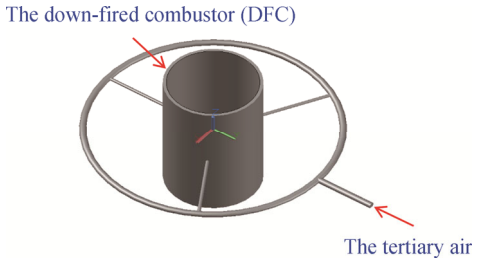

Fig. 2 Schematic diagram of the tertiary air nozzle

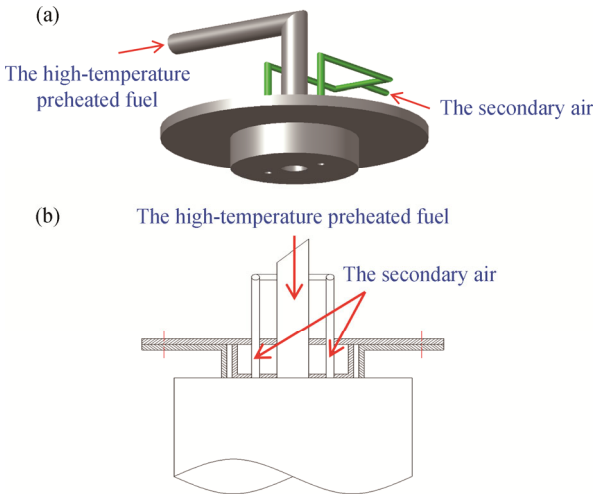

Fig. 3 Schematic diagram of the secondary air nozzle

The secondary air nozzle used in this experiment is shown in Fig. 3. In order to adjust fuel to achieve flameless combustion and low NO_x emissions, the high-temperature preheated fuel was injected into the central cylinder, while the secondary air was injected from symmetrical channels on both sides of the nozzle. The jet velocity of preheating fuel was between 10 m/s and 25 m/s, while the jet velocity of secondary air was between 10 m/s and 100 m/s.

2.2 Fuel characteristics

The fuel used in the experiments was Shenmu semi-coke produced in Shaanxi province of China, which was obtained by slow pyrolysis of Shenmu bituminous coal at 600°C–700°C. Proximate analysis of Shenmu semi-coke was determined according to *Proximate Analysis of Coal* (GB/T 212-2008). It could be inferred that the reason for the high moisture content of Shenmu semi-coke was the high moisture content of its raw coal. What's more, the pyrolysis semi-coke had a rich pore structure and large specific surface area, and hence there would be different degrees of moisture relapse phenomena during storage. Detected by Mastersizer 2000 laser analyzer, the particle size of Shenmu semi-coke was ranged from 0 to 0.1 mm, with 50% cut size (d_{50}) of 37.85 μm. The properties (proximate and ultimate analysis) of Shenmu semi-coke are exhibited in Table 2. As the bed material, quartz sand was added before the experiments began, with 0.10 mm to 0.50 mm particle size range.

Table 2 The properties of Shenmu semi-coke

Items	Data
Ultimate analysis/wt.% (air dry)	
Carbon (C_{ad})	68.31
Hydrogen (H_{ad})	0.85
Oxygen (O_{ad})	4.01
Nitrogen (N_{ad})	0.58
Sulfur (S_{ad})	0.3
Proximate analysis/wt.% (air dry)	
Moisture (M_{ad})	14.6
Ash (A_{ad})	11.36
Volatile matter (V_{ad})	7.31
Fixed carbon (FC_{ad})	66.72
Low heating value/MJ·kg^{-1}	23.32

2.3 Experimental conditions

Experimental conditions are shown in Table 3. Remaining unchanged and staying in a plateau, the fuel feed rate was 5.80 kg/h in the course of the experiment. A tertiary air was introduced at a distance of 1000 mm from the secondary air nozzle. The primary air ratio of the

self-preheating device (λ_P) and the ratio of total air to the theoretical combustion air (λ) remained unchanged, and solely the secondary air excess ratio (λ_2) was adjusted. The arrangement of low λ_p was to increase the heat load of the DFC, and the partial combustion heat release of Shenmu semi-coke in the self-preheating device was only to meet its own heating needs. O_2 concentration in the tail of the test rig hovered within the range of 3.0%–3.5%.

Table 3 Experimental conditions

Items	Unit	Case 1	Case 2	Case 3
Fuel feed rate	kg/h	5.80	5.80	5.80
Primary air	m^3/h	12.48	12.48	12.48
λ_p	–	0.35	0.35	0.35
Secondary air	m^3/h	7.08	14.16	18.36
λ_2	–	0.20	0.40	0.52
Tertiary air	m^3/h	23.04	16.02	12.04
λ_3		0.65	0.45	0.33
Total air	m^3/h	42.60	42.60	42.60
λ	–	1.20	1.20	1.20

Notes: λ_p-Ratio of the primary air to the theoretical combustion air, λ_2-Ratio of the secondary air to the theoretical combustion air, λ_3-Ratio of the tertiary air to the theoretical combustion air, λ-Ratio of the total air to the theoretical combustion air

3. Results and Discussion

3.1 The stability of the self-preheating device

The course of temperature varies with time in self-preheating device is demonstrated in Fig. 4. There were 5 temperature measuring points. Among them, T_1 to T_4 referred to the temperature at the bottom, middle, top of the riser and the loop-seal recycle device, respectively, while T_5 referred to the temperature at the exit of the cyclone separator. As Fig. 4 shows, the self-preheating device operated stably, with the highest temperature in dense phase zone (906°C) and the lowest temperature in the self-preheating device outlet (679°C). The heat released by Shenmu semi-coke was used to smoothly warm up itself and the surrounding material. After the material circulation was successfully established, the high-temperature preheated fuel would be supplied into the DFC continuously and smoothly.

In the course of the experiment, the gas components after preheating were sampled and analyzed by gas chromatography (Agilent 3000 A) with the instrument error of ±2%. Since the operating parameters were not transformed, the results of preheated gas composition under these three cases were consistent. The final analysis results are shown in Fig. 5. The major compositions of coal gas were N_2, CO_2, CO and H_2, and the concentration was 70.98%, 15.07%, 7.59% and 5.61%, respectively. The presence of O_2 and NO_x were not detected and no significant HCN was found, which meant that the coal gas had strong reducibility and had a good inhibitory effect on the generation of NO_x since the majority of the released fuel-N was converted into N_2 and NH_3 [37, 43–45], which was conducive to controlling the emission of NO_x from the overall system.

The particle size of high-temperature coal char (refers to the solid fuel of Shenmu semi-coke after being preheated) which was gathered at the cyclone separator outlet was detected and analyzed. Fig. 6 shows the size distribution of coal char (red dot plot) and raw fuel (hollow dot plot). By comparison with Shenmu semi-coke, the size distribution range of coal char was

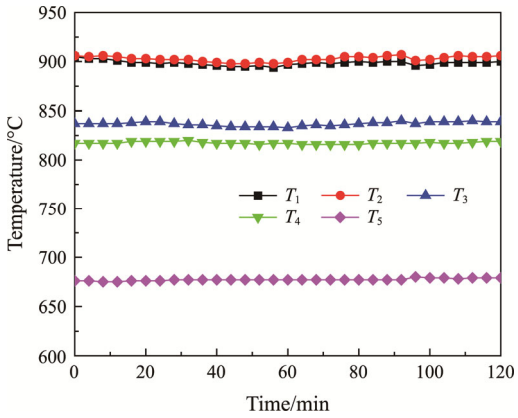

Fig. 4 Temperature variations over time in self-preheating device

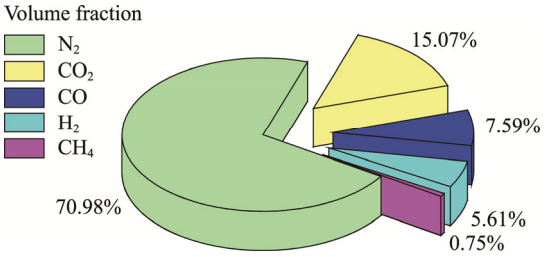

Fig. 5 Coal gas compositions at the outlet of the self-preheating device

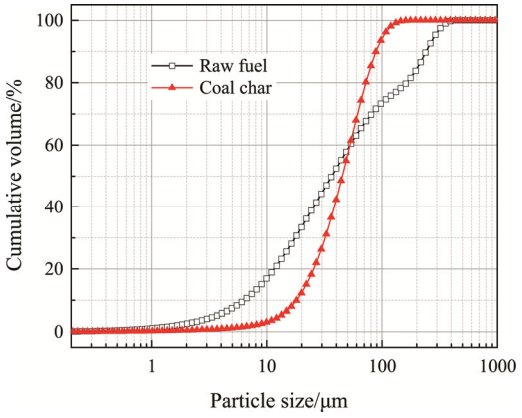

Fig. 6 Particle size distribution of the coal char and raw fuel

narrower, mainly concentrated in the range of 10 μm to 100 μm. For the factor that larger particles were gradually broken and burnt under thermal impact, while smaller particles were consumed in a direct way, leading to the highest proportion of particles of medium size. On the whole, the narrower the particle distribution range was, the larger the specific surface area was, which led to a better reactivity. Therefore, with the self-preheating, the combustion performance of coal char could be greatly improved to some extent.

Table 4 indicates the properties of the coal char. For the determined fuel, the proximate analysis of volatile matter, fixed carbon and ash content were stable values, which was to say, a certain amount of ash content must correspond to a certain quantity of fuel. In the process of thermal volatilization, the ash content of fuel always presented in the carbon residue and remained constant, thus ash content could be used for the tracer analysis. According to Eqs. (4) and (5) in literature [46], the conversion ratio (C_x) of each component of preheated fuel in the preheating process could be calculated as follows (combined with Table 2 and Table 4):

$$C_x = 1 - \frac{A_1 X_2}{A_2 X_1} \tag{1}$$

Table 4 Properties of the coal char

Items	Data
Ultimate analysis/wt.% (air dry)	
Carbon (C_{ad})	67.42
Hydrogen (H_{ad})	1.10
Oxygen (O_{ad})	4.23
Nitrogen (N_{ad})	0.82
Sulfur (S_{ad})	0.58
Proximate analysis/wt.% (air dry)	
Moisture (M_{ad})	1.52
Ash (A_{ad})	24.33
Volatile matter (V_{ad})	6.32
Fixed carbon (FC_{ad})	67.83

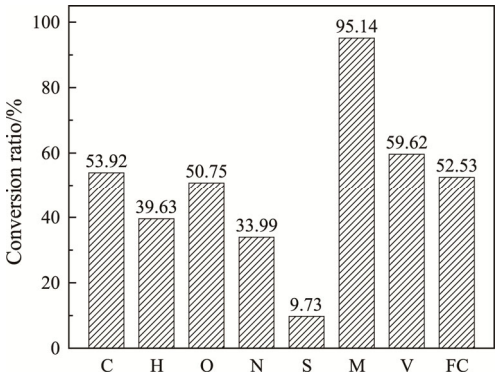

Fig. 7 Conversion ratio of each composition

where A_1 and A_2 are respectively the ash content of raw coal and the coal char (%); X_1 and X_2 represent the content of element or component x of raw coal and the coal char (%), respectively. Fig. 7 shows the conversion ratios of each composition during the preheating process.

In the course of the preheating process, the conversion ratios of each element and component were very high, the majority of which were above 50%. Therefore, it could be inferred that the precipitation and transformation of each component would play a vital role for the features of combustion and low NO_x emissions in the DFC. Both Table 4 and Fig. 7 could demonstrate that the atmosphere in the self-preheating device was strongly reductive, for the reason that the process of partial gasification and partial combustion took place rapidly. About 59.62% of the volatile matter was separated out; at the same time, more than 50% of carbon and oxygen elements were precipitated into the composition of high-temperature coal gas (Fig. 5). The conversion ratio of sulfur and nitrogen was the least, with rarely 9.73% and 33.99%, respectively. In Fig. 5, the precipitated N element was mainly converted into the inert gas (N_2), nevertheless, the majority of the nitrogen and sulfur elements remained in the coal char subsequently entered the DFC for continued combustion. To determine the distribution of nitrogen element in the high-temperature preheated fuel, moisture and volatile matter were removed from the collected coal char heated in a muffle furnace. According to mass conservation and the ash tracer method, nitrogen content of the remaining material after heating (ash & fixed carbon) was detected using EA 3000 high-accuracy elemental analyzer. Therefore, the content of volatile-N and char-N in the preheated fuel could be calculated accurately. The consequences are represented in Table 5. The proportion of char-N in total

Table 5 Distribution of nitrogen in the high-temperature preheated fuel

Items	Unit	Data
Total mass of sample (coal char)	g	1.00
M_R	g	0.92
N_s	wt.%	0.82
M_s	mg	8.20
N_R	wt.%	0.89
$M_{char\text{-}N}$	mg	8.19
$M_{volatile\text{-}N}$	mg	0.01
$W_{char\text{-}N}$	wt.%	99.88
$W_{volatile\text{-}N}$	wt.%	0.12

Notes: M_R-Remaining material mass (expulsion of moisture and volatile matter); N_s-Nitrogen (N_{ad}) content of coal char; M_s-Total mass of Nitrogen in coal char; N_R-Nitrogen (N_{ad}) content of remaining material; $M_{char\text{-}N}$-Total mass of nitrogen in remaining material; $M_{volatile\text{-}N}$-Total mass of nitrogen in volatile matter; $W_{char\text{-}N}$-The proportion of char-N in total nitrogen; $W_{volatile\text{-}N}$-The proportion of volatile-N in total nitrogen

nitrogen was significantly higher than that of volatile-N in total nitrogen. The nitrogen in the high-temperature preheated fuel (more favorable for combustion than raw fuel) mainly existed in the form of char-N (99.88%), and it was believed that there was basically no volatile matter involved in the combustion of the DFC, and char-N would be the main source of NO_x generation in the subsequent combustion.

3.2 Combustion characteristics of the high-temperature preheated fuel

Temperature profiles along the DFC are shown in Fig. 8. It was worth noting that temperatures transformed remarkably gently at 1000 mm (tertiary air injection), without any apparent fluctuation. What's more, when λ_2 was relatively low, slowly increasing λ_2 would have little effect on temperature; When λ_2 was relatively large, the influence of increasing λ_2 on temperature was significant. The temperature of the preheated fuel entering the DFC was 679°C; nevertheless, the first measurement point of the DFC (100 mm) was much higher. Hence, the temperature rose sharply within 0–100 mm of the DFC, of which the possible trigger was: (1) the preheated fuel injected into the DFC reacted with part of the secondary air, thus this homogeneous phase reacted quickly and had high heat release rate reaction; (2) the recirculation of the high-temperature flue gas given rise to high velocity air jet resulted in the high data of temperature measurement point. Below 100 mm of the DFC, the temperature and the thermal stability both had a decline to some extent due to the less air and external heat dissipation of the system. Additionally, the changes of subsequent temperature were most likely resulted from the burning of coal char. When λ_2 increased, the combustion zone of the secondary air nozzle (0–1000 mm) should contribute to more combustion, but the fact was not the case: the overall temperature profiles at the top of the DFC showed a downward trend. For the reason that more cold air poured into the DFC and absorbed a large amount of heat, affecting the combustion of preheated fuel at the top of the DFC, and hence finally showing a trend of temperature reduction. Above 1500 mm of the DFC, the temperature profiles were consistent. In other words, when the thermal load and the total air ratio kept constant, the effect of secondary air excess ratio was mainly reflected the temperature in the first half of the DFC, and when λ_2 was increased, the influence range was continuously expanded to the downstream. Therefore, in order to achieve more uniform temperature profiles, it was not feasible to convert λ_2 solely. Although blindly increasing λ_2 could expand its influence range, it would also excessively reduce the temperature at the top of the DFC, which was not worth the cost.

Images of the combustion process were captured with a digital camera along the DFC. The camera parameters were fixed (aperture 4, shutter 1/1000 s, ISO 1000) and Fig. 9 manifested the results. It was seen that with the increase of λ_2, the overall brightness of the combustion

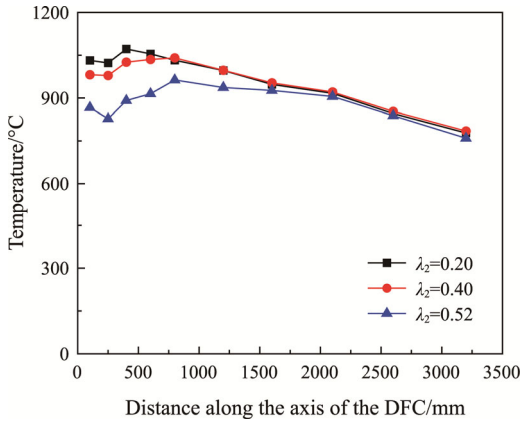

Fig. 8 Temperature profiles along the DFC

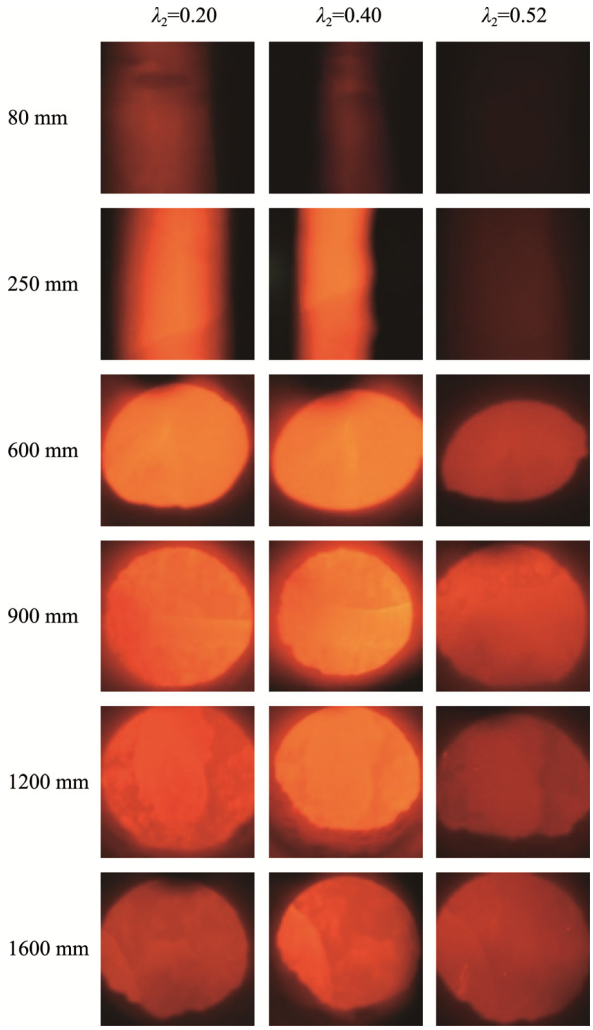

Fig. 9 Combustion images along the DFC

images was decreasing, and the color altered from dark yellow to dark red. The combustion zone was transparent and no flame fronts were seen.

In Kumar's research [47], the mean temperature, T_{mean}, which was calculated by averaging it over the cell residence times, was defined as the spatial mean temperature in the combustion zone and T' was defined as the mean square temperature fluctuation over the combustor. The specific formulas for computing them are as follows:

$$T_{mean} = \frac{\int T \mathrm{d}V}{\int \mathrm{d}V} \tag{2}$$

$$T' = \left[\frac{\int \left(\frac{T - T_{mean}}{T_{mean}} \right)^2 \mathrm{d}V}{\int \mathrm{d}V} \right]^{1/2} \tag{3}$$

The results in this experiment demonstrate that the spatial mean temperature of the DFC was 964°C, and the mean square temperature fluctuation was 10.65% when λ_2=0.20. While the spatial mean temperature of the main combustion area, which was defined as the zone from the secondary air nozzle to 1200 mm of the DFC, was 1063°C and the mean square temperature fluctuation was 2.18%. Obviously, due to the lower temperature of the DFC, the mean square temperature fluctuations of other two cases would be lower than Case 1. Refs. [46, 47] demonstrated that the mode of combustion could be made a definition as flameless combustion, provided that the normalized temperature fluctuation of the combustion mode was within 15% in a reactor. In this experiment, the mean square temperature fluctuations of the combustor were all less than 11%. Especially in the main combustion zone, the mean square temperature fluctuations of the combustor were even less than 3%, which strongly met Kumar's definition of flameless combustion. In the coal MILD combustion experiment of Li et al. [17], the true flameless combustion has never been observed and there were always sparks existing. Speculatively, this was because sparks were related to firing char particles. In this case, the big yellow flame appearing in the conventional case becomes invisible. Therefore, the volatile combustible gas was burning invisibly, while the droplets or char particles were just firing under the volatile MILD condition and remain visible. Smart et al. [18] and Weber et al. [30] also observed that the glow red particle was firing under the coal or sawdust MILD combustion. In this study, the combustion zone was transparent and no visible front flame existed, which was presumably caused by the relatively long residence time of fuel after being pretreated by the self-preheating device [43]. Since all cases with different λ_2 achieved flameless combustion, and the above different secondary air excess ratios were also basically in the common range of self-preheating combustion technology, λ_2 was not a decisive factor about whether the high-temperature preheated fuel could achieve flameless combustion.

The processing of the gray value of each combustion image was directly performed to draw the curve of gray value variation along the axis of the DFC under different λ_2, as shown in Fig. 10. Since the gray value of flame images could represent the brightness variation of the images to a large extent, Fig. 10 could also be seen as the image of the brightness variation of the DFC along which the brightness of high-temperature preheated fuel varied greatly at different positions. When λ_2 increased, the brightness of flame images at the top of the DFC decreased. The brightness of flame images in the DFC at 250–1600 mm was the most uniform when λ_2 was equal to 0.40.

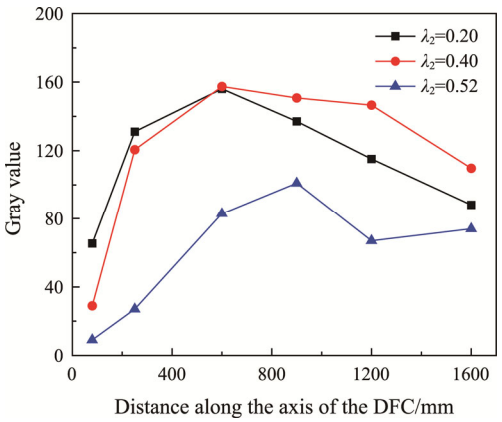

Fig. 10 Gray value of flame images along the DFC for different λ_2

In order to obtain regularities of combustion stability under the flameless combustion mode, the digital camera (fixed camera parameters) was used to shoot a series of flame videos, of which each frame was processed to gain in the same way by using MATLAB when the test rig was stably operating. Furthermore, the correlation value of every frame was calculated. The correlation value of the n-th frame (C_n) which represents the stability of flame and the intensity of combustion reaction, was described in detail in the literature [46, 48]. Reflecting the reaction strength of high-temperature preheated fuel (including combustion and gasification reaction), the fluctuation curves of brightness of flame images at different λ_2 are shown in Fig. 11, which can mainly reflect the stability characteristics of the combustion zone, including the stability of the flow process and the stability of the combustion process. The top of the DFC was the coal gas combustion area. Since the combustion process of coal

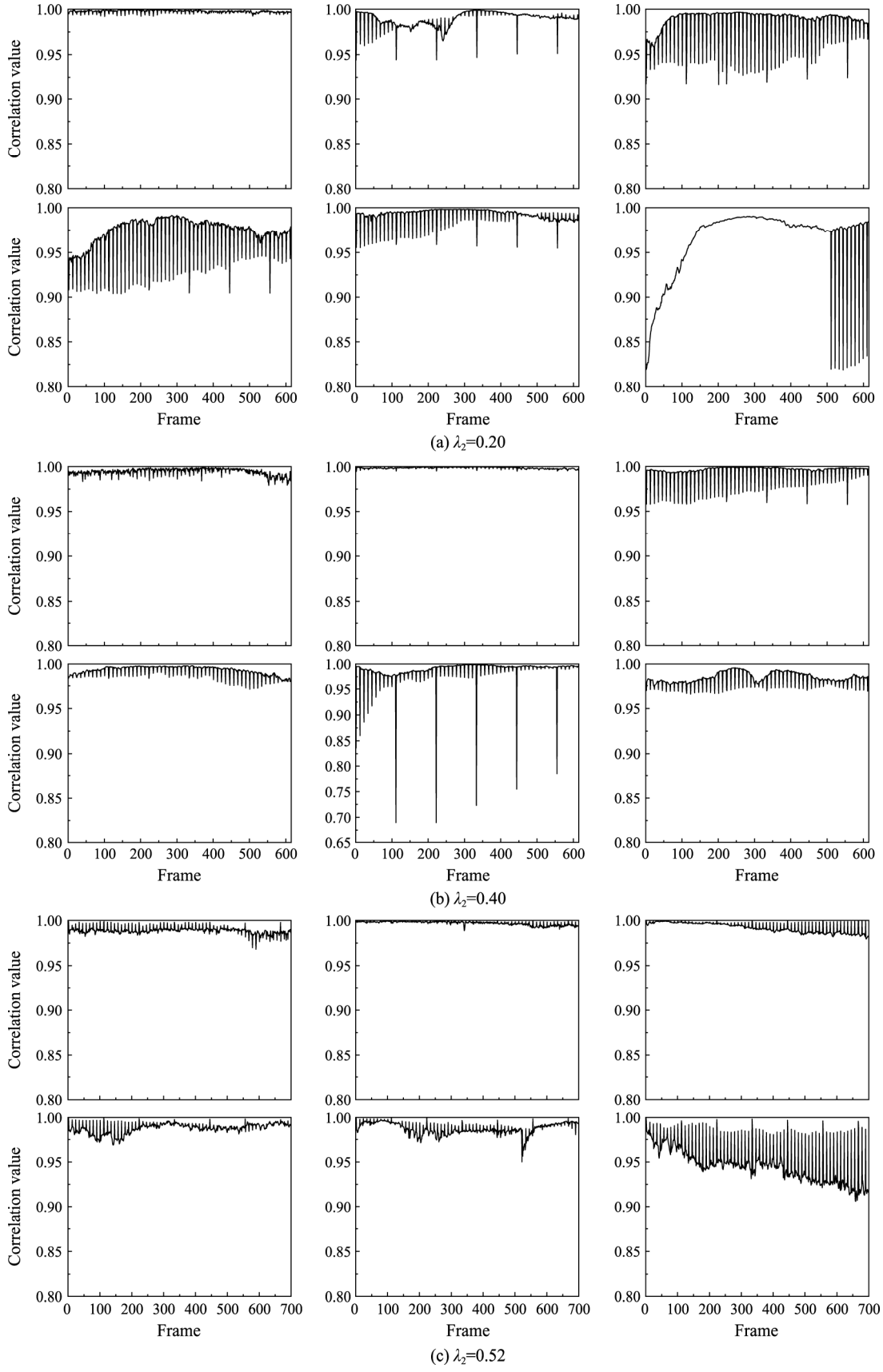

Fig. 11 Fluctuation curves of brightness of flame images at different positions in the DFC

gas was rapid and stable, the range of fluctuation curves became small. Nevertheless, the coal char's ignition and combustion in the midstream and downstream of the DFC relatively had a large fluctuation range due to the slower combustion process and the larger combustion area. The amplitude of the fluctuation curve gradually decreased with the increase of λ_2. To put it from another angle, the smaller λ_2 was, the more concentrated the combustion reaction was; the higher λ_2 was, the lower the reaction intensity was, and also the lower the temperature of combustion was.

The detailed formulas for computing combustion efficiency (η_c) can be expressed as follows:

$$\eta_c = 1 - q_3 - q_4 \tag{4}$$

$$q_3 = \frac{V_{gy} \times 123.36\text{CO}}{Q_{net,ar}} \times 100\% \tag{5}$$

$$q_4 = \frac{C_f}{100 - C_f} \times \frac{33\ 727\text{A}_{ar}}{Q_{net,ar}} \times 100\% \tag{6}$$

where q_3 is the gas incomplete combustion heat loss (CO), %; q_4 is the heat loss from solid incomplete combustion, %; V_{gy} is the volume of exit flue gas; C_f is the combustible percentage of fly ash.

According to Guo's research [49], the burnout ratio (η_b) of pulverized coal could be calculated based on the principle of ash equilibrium. The formula is as follows:

$$\eta = \left\{1 - \frac{\left[A_0 + \alpha(100 - \gamma)/100\right](100 - A)}{A(100 - A_0 - \alpha + \alpha\gamma/100)}\right\} \tag{7}$$

where A_0 is the ash content of Shenmu semi-coke (%); α is the addition amount of combustion-supporting agent (%); γ is the burning loss of combustion-supporting agent (%), and A is the ash content of the combustion residue.

The carbon contents of fly ash, burnout ratios and combustion efficiencies in different experimental cases are shown in Table 6. The carbon content of the exit fly ash measured at different λ_2 was 6.28%, 7.36% and 10.68%, respectively. The burnout ratios and combustion efficiencies of high temperature coal char were both large (all higher than 98%), which proved that self-preheating combustion technology could potentially realize the organic integration of efficient combustion and low NO_x emission. With the increase of λ_2, both burnout ratio and combustion efficiency showed a downward trend, which was because the overall combustion temperature in the DFC decreased with the increase of λ_2, resulting in a weakened combustion effect and intensity of the high temperature coal char. On the whole, efficient combustion has been achieved in all experimental cases.

Table 6 Carbon contents of fly ash, burnout ratios and combustion efficiencies

Items	Unit	Case 1	Case 2	Case 3
Burnout ratio	%	99.14	98.98	98.47
Carbon content of fly ash	%	6.28	7.36	10.68
Combustion efficiency	%	98.95	98.75	98.13

3.3 Flue gas analysis

A fourier infrared gas analyzer (GASMET Technologies Oy, Finland, instrument error<±2%) was deployed to gain the measurement of compositions of the flue gas along the axis of the DFC online. CO concentration variation along the axis of the DFC is presented in Fig. 12. The consequence revealed that CO concentration dropped sharply at the top of the DFC, and the concentration was low and substantially constant in the downstream. With increasing λ_2, the initial CO concentration was higher. Since the preheated fuel entering the DFC remained the same, it was taken into account that the difference in CO concentration was spawned by the gasification reaction in the DFC. When λ_2 increased, the high-temperature flue gas entrained by the increase of jet at a high rate; the combustion air was diluted to a greater extent, and the combustion reaction was weaker. The share of char and CO_2 gasification reaction increased; therefore the concentration of CO at the first measurement point was higher.

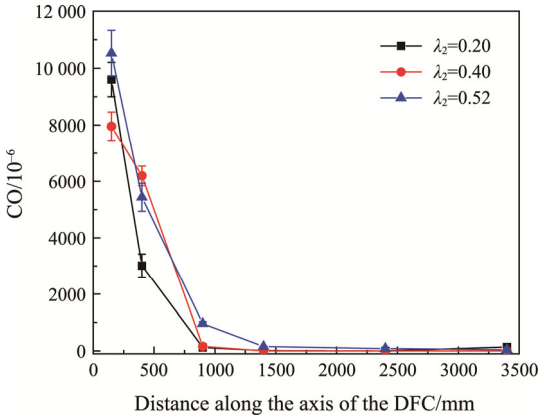

Fig. 12 CO concentration along the DFC

The Nitrogenous gas (not including N_2) in composition of high-temperature coal gas was mainly NH_3, the precursor of NO_x, which was decomposed into NH_2 at the beginning and subsequently produced NO through a series of reactions. The NH_3 concentration along the DFC with different λ_2 is shown in Fig. 13. It could be seen that the NH_3 concentration along the DFC had a universal low-level.

N_2O concentration along the DFC with different λ_2 is shown in Fig. 14. It manifested that N_2O concentration also had a basically low-level, and the formation of N_2O was greatly affected by combustion temperature. When the temperature in the DFC was below 900°C, N_2O concentration would probably have a higher level.

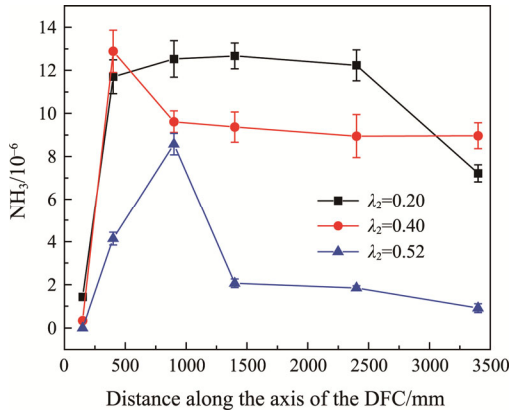

Fig. 13 NH_3 concentration along the DFC with different λ_2

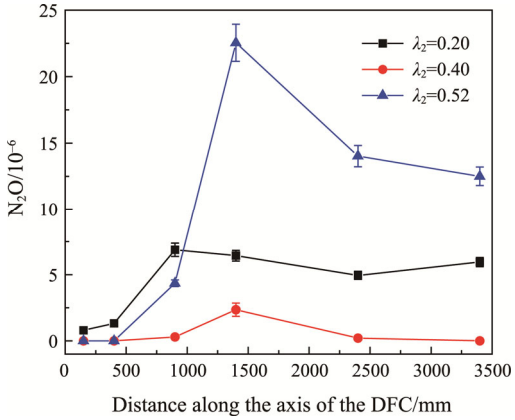

Fig. 14 N_2O concentration along the DFC with different λ_2

Fig. 15 and Fig. 16 illustrate NO_2 and NO concentration variations along the axis of the DFC, respectively. The result of NO_2 concentration measured at each measurement point was basically low, barely the top of the DFC had an insignificant amount of NO_2, of which the concentration was next to 0 in the downstream, so NO_x in the DFC was mainly presented in the form of NO. The concentration of NO_2 in the top of the DFC reached the highest, while compared with other measuring points, the highest concentration of CO was also found at the top measurement point, which indicated that the reducing atmosphere was the strongest. There are several reasons to illustrate this phenomenon. On the one hand, in a strong reducing atmosphere, fuel-N was easily converted to NO_2. According to Wang's research [50], a high level of CO would weaken the reduction effect of NO_2. Therefore, NO and NO_2 could be both detected at the top position of the DFC, but the concentration of NO_2 was significantly lower than NO. On the other hand, the combustion reaction became stronger in the range of 400 mm–500 mm of the DFC, resulting in the increase of CO consumption. Thus, a large amount of NO_2 would be gradually reduced in the atmosphere of low CO concentration, which led to the increase of NO at this time. In accordance with the literature [51], NO_2 was mainly generated in the fuel-rich region, and mainly converted into NO in the post-flame region. Its main generation and consumption reactions were [52]:

$$O+NO_2 \rightarrow NO+O_2 \quad (R1)$$

$$NO+HO_2 \rightarrow NO_2+OH \quad (R2)$$

$$H+NO_2 \rightarrow NO+OH \quad (R3)$$

When λ_2 was 0.20, the NO concentration continued to decrease. When λ_2 was 0.52, the NO concentration curve displayed a fluctuation greatly. It was seen that with increasing λ_2, the fluctuation of the NO concentration curve became greater. For the reason that the increase of λ_2 increased the jet momentum, which resulted in more high-temperature recirculating flue gas, and the recirculation region became wider. When λ_2 was 0.40, the overall NO concentration was the lowest. Below 900 mm of the DFC, the sharp drop in NO was mainly due to the dilution of tertiary air. The downstream NO was slowly decreasing. The decrease of NO in this area was mainly attributed to the heterogeneous reduction reaction of char. Combustion reaction is dominant above 400 mm of the DFC so that NO concentration rose rapidly again.

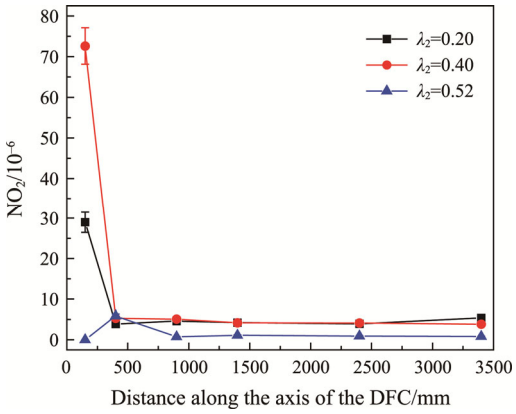

Fig. 15 NO_2 concentration along the DFC

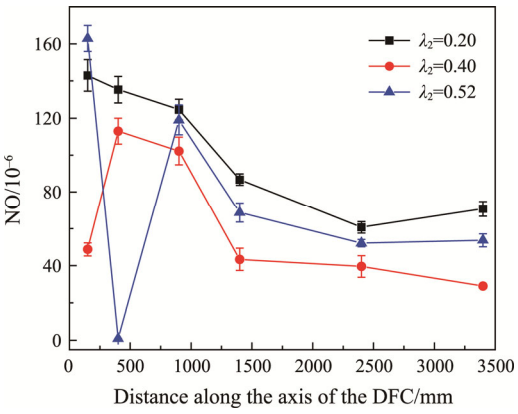

Fig. 16 NO concentration along the DFC

The exit NO_x and CO emissions are shown in Fig. 17. All data were converted to a standard value of 6% O_2

concentration. When λ_2 was 0.40, the NO_x emission was the lowest, and the value was 64.35 mg/m^3 (@6%O_2). It was concluded that NO_x emission did not vary linearly with λ_2. As λ_2 increased, the exit NO_x emission reached a decrease at the beginning and a increase thereafter. In the study of Fan et al. [53], Spliethoff et al. [54] and Yang et al. [55], NO_x emission at the outlet of the combustion equipment could be considerably reduced by air staging, and the reduction rate of NO_x was positively correlated with the degree of air staging. This was not consistent with the conclusion of this study. On the one hand, the fuel used in their studies contained high volatile contents. On the other hand, this study applied self-preheating combustion technology, which was essentially different from conventional direct combustion of pulverized coal. In conventional pulverized coal combustion, in addition to being advantageous for stable combustion, nitrogen in the volatiles was also a major source of NO_x. Therefore, by deep air staging, the nitrogen in the volatiles could be directionally reduced to N_2, thereby achieving the purpose of reducing NO_x. Nevertheless, in this study, the fuel used itself had a low volatile content, and a plenty of volatile matter was released in the course of the preheating process. Therefore, the purpose of air staging was to suppress the conversion of nitrogen in the char to NO_x, in addition to suppressing the conversion of the precursor into NO_x. On the other hand, in conventional pulverized coal combustion, with the purpose of stabilize the combustion of pulverized coal, the actual air equivalence ratio of the main combustion zone in their experiments was unlikely to be too small (generally higher than 0.65 [54, 55]). Therefore, there was no further discussion about the lower air excess ratio in reduction zone. According to the experimental results in this section, λ_2 was reasonably controlled serving the purpose of satisfying the low emission requirements of NO_x.

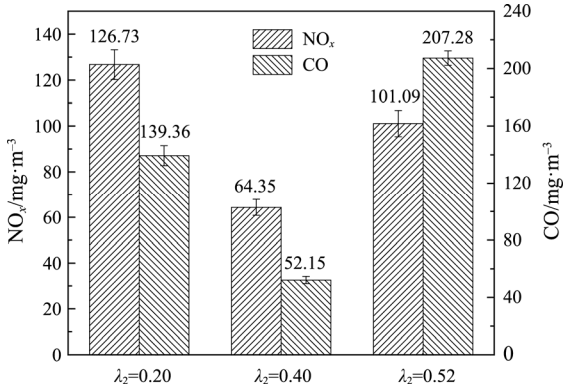

Fig. 17 NO_x and CO emissions

4. Conclusions

Some experiments attached importance to the effects of the secondary air excess ratio were initiated on a bench-scale combustion test rig. The optimal secondary air excess ratio corresponding to the lowest NO_x emissions has been determined. Aiming at semi-coke combustion issue and environmental protection requirement, this study was beneficial to optimize the design and operation for self-preheating combustion technology and reduce NO_x emissions further, which provided the experimental and theoretical basis for industrial application. The detailed conclusions could be summarized as follows:

(1) The NO_x at the top of the combustor was mainly generated by the nitrogen-containing substances in coal gas which had strong reducibility and had a good inhibitory effect on the generation of NO_x as the majority of the released fuel-N was converted to NH_3 and N_2.

(2) The rapid ignition of coal gas and the recirculation of high-temperature flue gas resulted in relatively high combustion temperatures close to the preheated fuel nozzle exit. Increasing λ_2 would excessively reduce the temperature at the top of the DFC.

(3) All cases with different λ_2, basically in the common range of self-preheating combustion technology, achieved flameless combustion. λ_2 was not a decisive factor about whether the high-temperature preheating fuel could achieve flameless combustion.

(4) With λ_2 increasing, the exit NO_x emission was not reduced linearly, which was dissimilar from conventional air staging combustion. The volatile-N was released in the self-preheating device, and a large portion of NO_x was generated from char-N, which was hard to effectively reduce under deep air staging condition. Instead, it was necessary to get command of the mixing process of preheated fuel and air, and succeeding control the release rate of char-N.

(5) The unburned carbon content of the fly ash reached a slight increase with λ_2 increasing, and all the combustion efficiencies were generally exceeded 98%. λ_2 was reasonably controlled serving the purpose of satisfying the low emission requirements of NO_x. When λ_2 was the optimum value of 0.40, the lowest NO_x emission was 64.35 mg/m^3 (@6% O_2).

Acknowledgment

This study was supported by Strategic Priority Research Program of the CAS (XDA29010200), CAS Project for Young Scientists in Basic Research (YSBR-028), and Youth Innovation Promotion Association of the CAS (2019148).

References

[1] Li Z., Liu G., Zhu Q., Chen Z., Ren F., Combustion and NO_x emission characteristics of a retrofitted down-fired 660 MWe utility boiler at different loads. Applied Energy,

2011, 88(7): 2400–2406.

[2] Kuang M., Li Z., Zhang Y., Chen X., Jia J., Zhu Q., Asymmetric combustion characteristics and NO_x emissions of a down-fired 300 MWe utility boiler at different boiler loads. Energy, 2012, 37(1): 580–590.

[3] Vodicka M., Hrdlicka J., Skopec P., Experimental study of the NO_x reduction through the staged oxygen supply in the oxy-fuel combustion in a 30 kWth bubbling fluidized bed. Fuel, 2021, 286: 119343.

[4] Ma S., Chai J., Jiao K., et al., Environmental influence and countermeasures for high humidity flue gas discharging from power plants. Renewable and Sustainable Energy Reviews, 2017, 73: 225–235.

[5] Zhang Y., Zhu J., Lyu Q., Liu J., Pan F., Zhang J., The ultra-low NO_x emission characteristics of pulverized coal combustion after high temperature preheating. Fuel, 2020, 277: 118050. https://doi.org/10.1016/j.fuel.2020.118050

[6] Ribeirete A., Costa M., Detailed measurements in a pulverized-coal-fired large-scale laboratory furnace with air staging. Fuel, 2009, 88(1): 40–45.

[7] Staiger B., Unterberger S., Berger R., et al., Development of an air staging technology to reduce NO_x emissions in grate fired boilers. Energy, 2005, 30(8): 1429–1438.

[8] Coda B., Kluger F., Fortsch D., et al., Coal-nitrogen release and NO_x evolution in air-staged combustion. Energy & Fuels, 1998, 12(6): 1322–1327.

[9] Chae J.O., Chun Y.N., Effect of two-stage combustion on NO_x emissions in pulverized coal combustion. Fuel, 1991, 70(6): 703–707.

[10] Lyu Q., Li S., Huang C., Current situation and development suggestions of coal clean and efficient combustion technology in industry field. Bulletin of Chinese Academy of Sciences, 2019, 34(4): 392–400.

[11] Hu Z., Jiang E., Ma X., Numerical simulation on operating parameters of SNCR process in a municipal solid waste incinerator. Fuel, 2019, 245: 160–173.

[12] Zhang L., Dong X., Hou F., et al., Study on optimization experiment of SCR denitrification technologies in a coal-fired power plant. IOP Conference Series: Earth and Environmental Science, 2018, 108(5): 052100.

[13] Liu C., Hui S., Pan S., Wang D., Shang T., Liang L., The influence of air distribution on gas-fired coal preheating method for NO emissions reduction. Fuel, 2015, 139: 206–212.

[14] Stadler H., Christ D., Habermehl M., et al., Experimental investigation of NO_x emissions in oxy-coal combustion. Fuel, 2011, 90(4): 1604–1611.

[15] Vascellari M., Cau G., Influence of turbulence-chemical interaction on CFD pulverized coal MILD combustion modeling. Fuel, 2012, 101: 90–101.

[16] Mei Z., Li P., Wang F., Zhang J., Mi J., Influences of reactant injection velocities on moderate or intense low-oxygen dilution coal combustion. Energy & Fuels, 2014, 28(1): 369–384.

[17] Li P., Wang F., Tu Y., et al., Moderate or intense low-oxygen dilution oxy-combustion characteristics of light oil and pulverized coal in a pilot-scale furnace. Energy & Fuels, 2014, 28(2): 1524–1535.

[18] Smart J.P., Riley G.S., Combustion of coal in a flameless oxidation environment under oxy-fuel firing conditions: the reality. Journal of the Energy Institute, 2012, 85(3): 131–134.

[19] Mei Z., Li P., Mi J., Wang F., Zhang J., Diffusion MILD combustion of firing pulverized-coal at a pilot furnace. Flow, Turbulence Combustion, 2015, 95: 803–829.

[20] Weidmann M., Honoré D., Verbaere V., Boutin G., Grathwohl S., Godard G., Gobin C., Kneer R., Scheffknecht G., Experimental characterization of pulverized coal MILD flameless combustion from detailed measurements in a pilot-scale facility. Combustion and Flame, 2016, 168: 365–377.

[21] Saha M., Dally B.B., Medwell P.R., Chinnici A., Burning characteristics of Victorian brown coal under MILD combustion conditions. Combustion and Flame, 2016, 172: 252–270.

[22] Saha M., Dally B.B., Chinnici A., Medwell P.R., Effect of co-flow oxygen concentration on the MILD combustion of pulverized coal. Fuel Processing Technology, 2019, 193: 7–18.

[23] Mao Z., Zhang L., Zhu X., et al., Investigation on coal moderate or intense low-oxygen dilution combustion with high-velocity jet at pilot-scale furnace. Applied Thermal Engineering, 2017, 111: 387–396.

[24] Mao Z., Zhang L., Zhu X., Zheng C., Experiment investigation of coal MILD-oxy combustion integrated with flue gas recirculation at a 0.3 MWth furnace. Fuel Processing Technology, 2017, 162: 126–134.

[25] Saha M., Dally B.B., Medwell P.R., Chinnici A., Effect of particle size on the MILD combustion characteristics of pulverized brown coal. Fuel Processing Technology, 2017, 155: 74–87.

[26] Perrone D., Castiglione T., Klimanek A., et al., Numerical simulations on oxy-MILD combustion of pulverized coal in an industrial boiler. Fuel Processing Technology, 2018, 181: 361–374.

[27] Hu F., Li P., Zhang T., Li W., Wang K., Guo J., Mi J., Liu Z., Reaction characteristics and MILD combustion of residual char in a pilot-scale furnace. Energy & Fuels, 2019, 33(12): 12791–12800.

[28] Wang X., Zhang J., Xu X., Mikulcic H., Li Y., Zhou Y., Tan H., Numerical study of biomass co-firing under oxy-MILD mode. Renewable Energy, 2020, 146: 2566–2576.

[29] Kuang Y., He B., Tong W., et al., Numerical simulation of

pulverized coal MILD-oxy combustion under different oxygen concentrations. Journal of the Energy Institute, 2020, 93(4): 1713–1725.

[30] Weber R., Smart J.P., Kamp W., On the (MILD) combustion of gaseous, liquid, and solid fuels in high temperature preheated air. Proceedings of the Combustion Institute, 2005, 30(2): 2623–2629.

[31] Mancini N.S., Mancini M., Szlek A., Weber R., Novel conceptual design of a supercritical pulverized coal boiler utilizing high temperature air combustion (HTAC) technology. Energy, 2010, 35(7): 2752–2760.

[32] Xing X., Wang B., Lin Q., Structure of reaction zone of normal temperature air flameless combustion in a 2 ton/h coal-fired boiler furnace. Proceedings of the Institution of Mechanical Engineers, Part A: Journal of Power and Energy, 2007, 221(4): 473–480.

[33] Dally B.B., Shim S.H., Craig R.A., Ashman P.J., Szego G.G., On the burning of sawdust in a MILD combustion furnace. Energy & Fuels, 2010, 24(6): 3462–3470.

[34] Rabovitser J., Bryan B, Nester S., Wohadlo S., Methane de- NO_x for utility PC boilers. Institute of Gas Technology (IGT), Des Plaines, USA, 2002.

[35] Rabovitser J., Bryan B, Knight R, Nester S., Wohadlo S., Development and testing of a novel coal preheating technology for NO_x reduction from pulverized coal-fired boilers. Proceedings of the Proceedings of 2003 Mega Symposium, Washington, 2003.

[36] Yao Y., Zhu J., Lyu Q. Experimental study on nitrogen transformation in combustion of pulverized semi-coke preheated in a circulating fluidized bed. Energy & Fuels, 2015, 29(6): 3985–3991.

[37] Ouyang Z., Ding H., Liu W., Cao X., Zhu S., Effect of the primary air ratio on combustion of the fuel preheated in a self-preheating burner. Combustion Science and Technology, 2022, 194(6): 1247–1264.

[38] Zhu S., Lyu Q., Zhu J., Wu H., Wu G., Effect of air distribution on NO_x emissions of pulverized coal and char combustion preheated by a circulating fluidized bed. Energy & Fuels, 2018, 32(7): 7909–7915.

[39] Zhu S., Lyu Q., Zhu J., Liang C., Experimental study on NO_x emissions of pulverized bituminous coal combustion preheated by a circulating fluidized bed. Journal of the Energy Institute, 2018, 92(2): 247–256.

[40] Ouyang Z., Liu W., Man C., Zhu J., Liu J., Experimental study on combustion, flame and NO_x emission of pulverized coal preheated by a preheating burner. Fuel Processing Technology, 2018, 179: 197–202.

[41] Man C., Zhu J., Ouyang Z., Liu J., Lyu Q., Experimental study on combustion characteristics of pulverized coal preheated in a circulating fluidized bed. Fuel Processing Technology, 2018, 172: 72–78.

[42] Liu W., Ouyang Z., Cao X., Na Y., Liu D., Zhu S., Effects of secondary air velocity on NO emission with coal preheating technology. Fuel, 2019, 256: 115898.

[43] Ouyang Z., Ding H., Liu W., Li S., Cao X., Effect of the staged secondary air on NO_x emission of pulverized semi-coke flameless combustion with coal preheating technology. Fuel, 2021, 291: 120137.

[44] Ding H., Ouyang Z., Zhang X., Zhu S., The effects of particle size on flameless combustion characteristics and NO_x emissions of semi-coke with coal preheating technology. Fuel, 2021, 297: 120758.

[45] Liu W., Ouyang Z., Cao X., Na Y., The influence of air-stage method on flameless combustion of coal gasification fly ash with coal self-preheating technology. Fuel, 2019, 235: 1368–1376.

[46] Liu W., Ouyang Z., Cao X., Na Y., Experimental research on flameless combustion with coal preheating technology. Energy & Fuels, 2019, 32(6): 7132–7141.

[47] Kumar S., Paul P.J., Mukunda H.S., Studies on a new high-intensity low-emission burner. Proceedings of the Combustion Institute, 2002, 29: 1131–1137.

[48] Shen S., Yu C., Yuan F., Chen Z., Zhang Y., Renovated method for identifying fire plume based on image correlation. Journal of Safety and Environment, 2007, 6: 96–99.

[49] Guo X., Wei G., Zhou Y., Ma Z., Ding Z., Shen F., Effect of MgO addition on burnout rate of pulverized coal for blast furnace injection. Iron and Steel, 2011, 46(7): 7–9.

[50] Wang C., Wang P., Du Y., Che D., Experimental study on effects of combustion atmosphere and coal char on NO_2 reduction under oxy-fuel condition. Journal of the Energy Institute, 2019, 92(4): 1023–1033.

[51] He R., Suda T., Takafuji M., Analysis of low NO emission in high temperature air combustion for pulverized coal. Fuel, 2004, 83(9): 1133–1141.

[52] Courtemanche B., Levendis Y.A., A laboratory study on the NO, NO_2, SO_2, CO and CO_2 emissions from the combustion of pulverized coal, municipal waste plastics and tires. Fuel, 1998, 77(3): 183–196.

[53] Fan W., Lin Z., Kuang J., Li Y., Impact of air staging along furnace height on NO_x emissions from pulverized coal combustion. Fuel Processing Technology, 2010, 91(6): 625–634.

[54] Spliethoff H., Greul U., Rudiger H., Hein K.R.G., Basic effects on NO_x emissions in air staging and reburning at a bench-scale test facility. Fuel, 1996, 75(5): 560–564.

[55] Yang J., Sun R., Sun S., Zhao N., Hao N., Chen H., Wang Y., Guo H., Meng J., Experimental study on NO_x reduction from staging combustion of high volatile pulverized coals. Part 1. Air staging. Fuel Processing Technology, 2014, 126: 266–275.